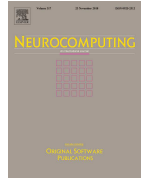




Preprint  
submitted to Elsevier



# Exclusive Independent Probability Estimation using Deep 3D Fully Convolutional DenseNets for IsoIntense Infant Brain MRI Segmentation

Seyed Raein Hashemi<sup>a,b,\*\*</sup>, Sanjay P. Prabhu<sup>a</sup>, Simon K. Warfield<sup>a</sup>, Ali Gholipour<sup>a</sup>

<sup>a</sup>Radiology Department, Boston Children's Hospital; and Harvard Medical School

<sup>b</sup>College of Computer and Information Science, Northeastern University

## ABSTRACT

**Background and Objective:** The most recent fast and accurate image segmentation methods are built upon fully convolutional deep neural networks. In particular, densely connected convolutional neural networks have shown excellent performance in detection and segmentation tasks. Infant brain MRI tissue segmentation is a complex segmentation task as the white matter and gray matter of the developing brain at about 6 months of age show similar T1 and T2 relaxation times, thus appear to have similar intensity values on both T1- and T2-weighted MRI scans. Brain tissue segmentation in this period is, therefore, very challenging. In this paper, we propose new deep learning strategies to overcome the challenges of isointense infant brain MRI tissue segmentation.

**Methods:** We propose new training strategies to train powerful 3D multi-channel fully convolutional deep DenseNets for isointense tissue segmentation. We introduce an exclusive multi-label training method to independently segment the mutually exclusive brain tissues with similarity loss function parameters that are balanced based on class prevalence. Using our proposed training technique based on similarity loss functions and patch prediction fusion we decrease the number of parameters in the network, reduce the complexity of the training process focusing the attention on less number of tasks, while mitigating the effects of data imbalance between labels and inaccuracies near patch borders.

**Results:** By taking advantage of these strategies we were able to perform fast image segmentation (less than 90 seconds per 3D volume), using a network with less parameters than many state-of-the-art networks (1.4 million parameters), overcoming issues such as 3D vs 2D training and large vs small patch size selection, while achieving the top performance in segmenting brain tissue among all methods tested in first and second round submissions of the 2017 MICCAI iSeg grand challenge.

**Conclusion:** We present a new and powerful 3D FC-DenseNet architecture, a novel exclusive multi-label patch-wise training technique with balanced similarity loss functions and a patch prediction fusion strategy that can be used on new classification and segmentation applications with two or more very similar classes. This strategy improves the training process by reducing its complexity while providing a trained model that works for any size input and is fast and more accurate than many state-of-the-art methods.

© 2018 Elsevier B.V. All rights reserved.

## 1. Introduction

Deep convolutional neural networks have shown great potential in medical imaging on account of dominance over traditional methods in applications such as segmentation of neu-

roanatomy [2, 14, 22, 3], lesions [18, 1, 11, 6], and tumors [7, 15, 19] using voxelwise networks [14, 7, 16, 17], 3D voxelwise networks [3, 11] and Fully Convolutional Networks (FCNs) [4, 13, 16, 17, 6]. FCNs have shown better performance while also being faster in training and testing than voxelwise methods [16, 17].

Recently, a new densely connected network called DenseNet [9] and a few of its extensions, such as a 3D

\*\*Corresponding author:

*e-mail:* Hashemi.s@husky.neu.edu (Seyed Raein Hashemi)

version called DenseSeg [2] and a fully convolutional two-path edition (FC-DenseNet) [10], showed promising results in image segmentation tasks [5], including the DenseSeg showing the top performance in the 2017 MICCAI isointense infant brain MRI segmentation (iSeg) grand challenge<sup>1</sup>, which is considered a very difficult image segmentation task for both traditional and deep learning approaches.

During early infant brain maturation through the myelination process, there is an isointense period in which the T1 and T2 relaxation times of the white matter (WM) and gray matter (GM) tissue become similar, resulting in isointense (similar intensity) appearance of tissue on both T1-weighted and T2-weighted MRI contrasts. This happens around 6 months of age where tissue segmentation methods that are based directly on image intensity are prone to fail [20]. Deep learning methods, however, have shown promising results in this application.

In this work, we aimed to further improve image segmentation under these challenging conditions. While the top performing methods in the iSeg challenge relied on the power of DenseNets and used conventional training strategies based on cross-entropy loss function [2, 5], in this work we focused on the training part and developed new strategies that helped us achieve the best performance currently reported on the iSeg challenge among all first<sup>2</sup> and second round submissions<sup>3</sup>. We built our technique over a deep 3D two-channel fully convolutional DenseNet; and trained it purposefully using our proposed multi-label multi-class method of training, with exclusively adjusted similarity loss functions on large overlapping 3D image patches. We overcame class similarity issues by focusing the training on one of the isointense class labels (WM) instead of both (thus referred to as exclusive multi-label multi-class), where we balanced precision and recall separately for each class using  $F_\beta$  loss functions [6] with  $\beta$  values adjusted based on class prevalence in the training set.

Our contributions that led to improved iso-intense image segmentation include 1) exclusive multi-label multi-class training (through exclusive independent probability estimation) using similarity loss functions; 2) using a 3D FC-DenseNet architecture adopted from [10] that is deeper than previous studies; and 3) training and testing on large overlapping 3D image patches with a patch prediction fusion strategy [6] that enabled intrinsic data augmentation and improved segmentation in the patch borders. Similarity loss functions, such as the Dice similarity loss, were previously proposed for two-class segmentation in V-Net [13]. The  $F_\beta$  loss functions, which showed excellent performance in training deep networks for highly imbalanced medical image segmentation [6], appeared to be effective also in multi-label training of DenseNets for multi-class segmentation in this work, where we adjusted the class imbalance hyper-parameter  $\beta$  directly based on training data in the training phase.

The official results on iSeg test data show that our method outperformed all previously published and reported methods improving DenseNets while standing in the first place after the second round submissions as of September 2018. Our proposed training strategy can potentially be used and extended

to other applications for multi-class segmentation and detection with two or more very similar and unbalanced classes. After a brief technical description of the isointense infant brain MRI segmentation challenge in the Motivation, the details of the methods, including the network architecture and our proposed strategies for training are presented in the Methods section; and are followed by the Results and the Conclusion sections.

## 2. Motivation

The publicly available MICCAI grand challenge on 6-month infant brain MRI segmentation (iSeg) dataset contains pre-processed T1- and T2-weighted MR images of 10 infant subjects with manual labels of cerebrospinal fluid (CSF), WM, and GM for training and 13 infant subjects without labels for testing. The intensity distribution of all classes (CSF, GM, WM) is shown in Figure 1, which shows that the intensity values of GM and WM classes on both MRI scans largely overlap. The GM-WM isointense appearance only happens around this stage of brain maturation and hinders GM-WM segmentation. CSF, which shows less overlap with GM and WM, shows a relatively spread intensity distribution, which is partly attributed to partial voluming effects in relatively large voxels where signal is averaged in the interface of GM and CSF, and because of the inclusion of some other non-brain tissue such as blood vessels in the CSF label in expert manual segmentation of the iSeg data.

In the iSeg training data, the number of voxels in each class label is different and can be roughly presented as the average ratio of (36, 1, 2, 1.5) for non-brain, CSF, GM, and WM classes, respectively. Unbalanced labels can make the training process converge to local minima resulting in sub optimal performance. The predictions, thus, may lean towards the GM class especially when distinguishing between the isointense areas of GM and WM. Using our proposed multi-label multi-class training method, which can be extended to other segmentation or detection tasks with very similar (isointense) while exclusive labels (each voxel belonging to a single label), we aimed to 1) let the network focus on and learn one of the segmentation challenges at a time rather than two (in this case WM rather than both GM and WM) reducing the number of training parameters, 2) reduce the bias in training on classes with higher occurrences (in this case GM), and 3) use balanced similarity loss functions on non-similar classes (in this case WM and CSF).

## 3. Methods

### 3.1. Network architecture

#### 3.1.1. DenseNets

In traditional densely connected networks each layer is connected to every other layer to preserve both high- and low-level features, in addition to allowing the gradients to flow from bottom layers to top layers resulting in more accurate predictions.

<sup>1</sup><http://iseg2017.web.unc.edu/>

<sup>2</sup><http://iseg2017.web.unc.edu/rules/results>

<sup>3</sup><http://iseg2017.web.unc.edu/evaluation-on-the-second-round-submission>

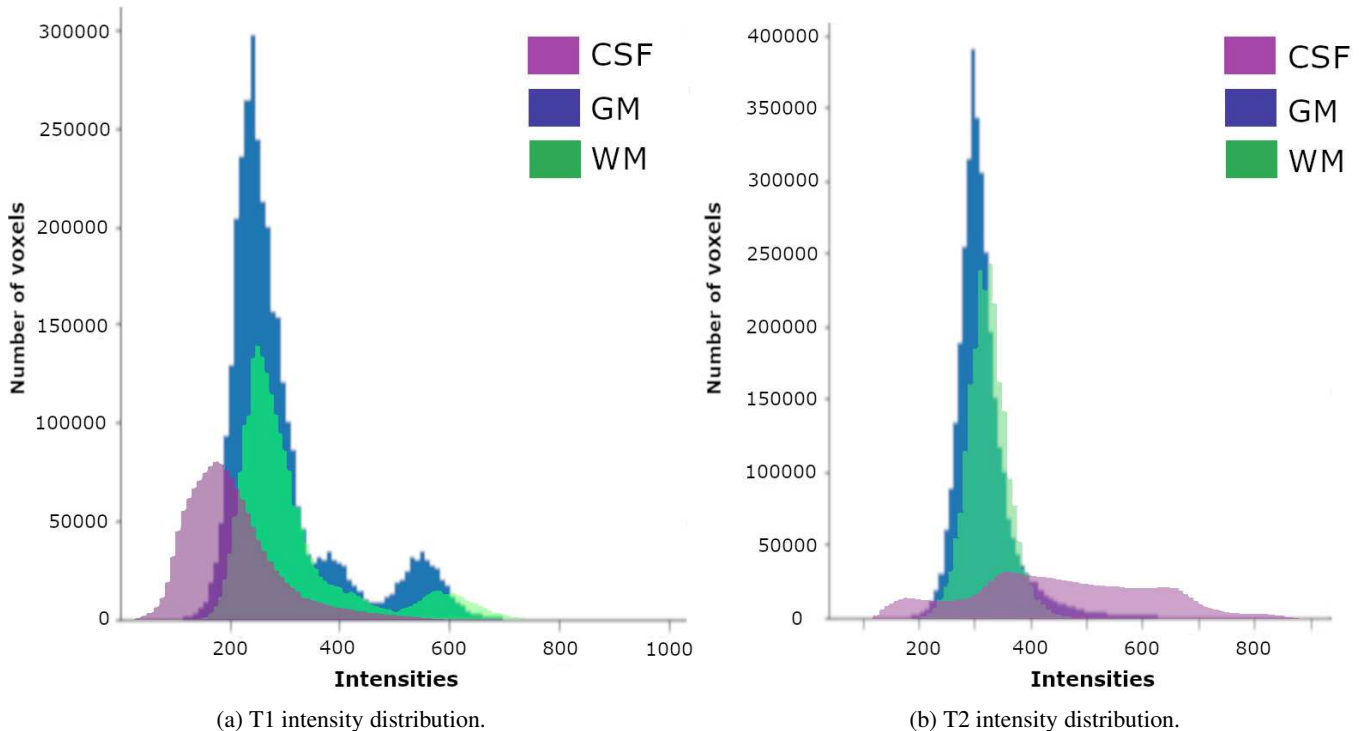


Fig. 1: Intensity distributions of all three classes on T1-weighted (on the left) and T2-weighted (on the right) MRI scans on all images in the iSeg training set. At 6 months of age, the intensity values of the white matter (WM) and gray matter (GM) in the infant brain, considered in iSeg, largely overlap. This makes WM-GM segmentation on these images very challenging. The cerebrospinal fluid (CSF), overall, shows better separation from WM and GM based on image intensity values.

Unlike Resnets [8] which only sum the output of the identity function at each layer with a skip connection from the previous layer:

$$x_l = H_l(x_{l-1}) + x_{l-1} \quad (1)$$

DenseNets [9] significantly improve the flow of information throughout the network by 1) using concatenation instead of summation and 2) forward connections from all preceding layers rather than just a previous layer, therefore:

$$x_l = H_l([x_0, x_1, \dots, x_{l-1}]) \quad (2)$$

where  $x$  is the output of the  $l^{\text{th}}$  layer,  $H_l$  is the  $l^{\text{th}}$  layer transition, and  $[x_0, x_1, \dots, x_{l-1}]$  refers to the concatenation of all previous feature maps.

### 3.1.2. Fully Convolutional 3D DenseNets

We designed our deep 3D densely connected network based on a combination of DenseSeg [2] and FC-DenseNet [10] architectures. This deep DenseNet [9] style architecture is shown in Figure 2 consisting of contracting and expanding paths. The network is trained on local features in the contracting path concatenated with upsampled global features in the expanding path. For this reason, the model has the capacity to learn both high-resolution local and low-resolution global 3D features.

The contracting path contains an initial  $2 \times 2 \times 2$  convolution with stride 2 for the purpose of reducing the patch size while preserving field of view. It is then followed by three padded  $3 \times 3 \times 3$  convolutional layers. Five dense blocks follow with a growth rate of 12. Growth rate for dense blocks is the increase amount in the number of feature maps after each block.

Dense blocks contain four  $3 \times 3 \times 3$  convolutional layers preceding with  $1 \times 1 \times 1$  convolutions which are known as bottlenecks [9]. Dimension reduction of 0.5 applied at transition layers also helps parameter-efficiency and reduce the number of input feature maps. There are skip connections between each and every layer inside dense blocks. Aside from the center dense block connecting the two paths, contracting dense blocks are followed by a  $1 \times 1 \times 1$  convolutional layer and a max pooling layer referred to as transition down blocks [9], and expanding dense blocks are preceded with a  $3 \times 3 \times 3$  transpose convolution with stride 2 also known as transition up blocks [10]. All convolutional layers in the network are followed by batch normalization and ReLU non-linear layers. Dropout rate of 0.2 is used only after  $3 \times 3 \times 3$  convolutional layers of each dense block. As the final layer a  $1 \times 1 \times 1$  convolution with a sigmoid or softmax output is used, as will be discussed later.

### 3.2. Training strategy

While our deep two-channel 3D fully convolutional DenseNet architecture used two extra downsampling and up-sampling convolutional layers to preserve the higher field of view, in this work we mainly focused on innovative training strategies to facilitate network training and improve results. These innovations include the use of similarity loss functions in particular  $F_\beta$  [6], using two different training approaches: single-label multi-class and exclusive multi-label multi-class training, use of large image patches as input, and a patch prediction fusion strategy, which are discussed here.

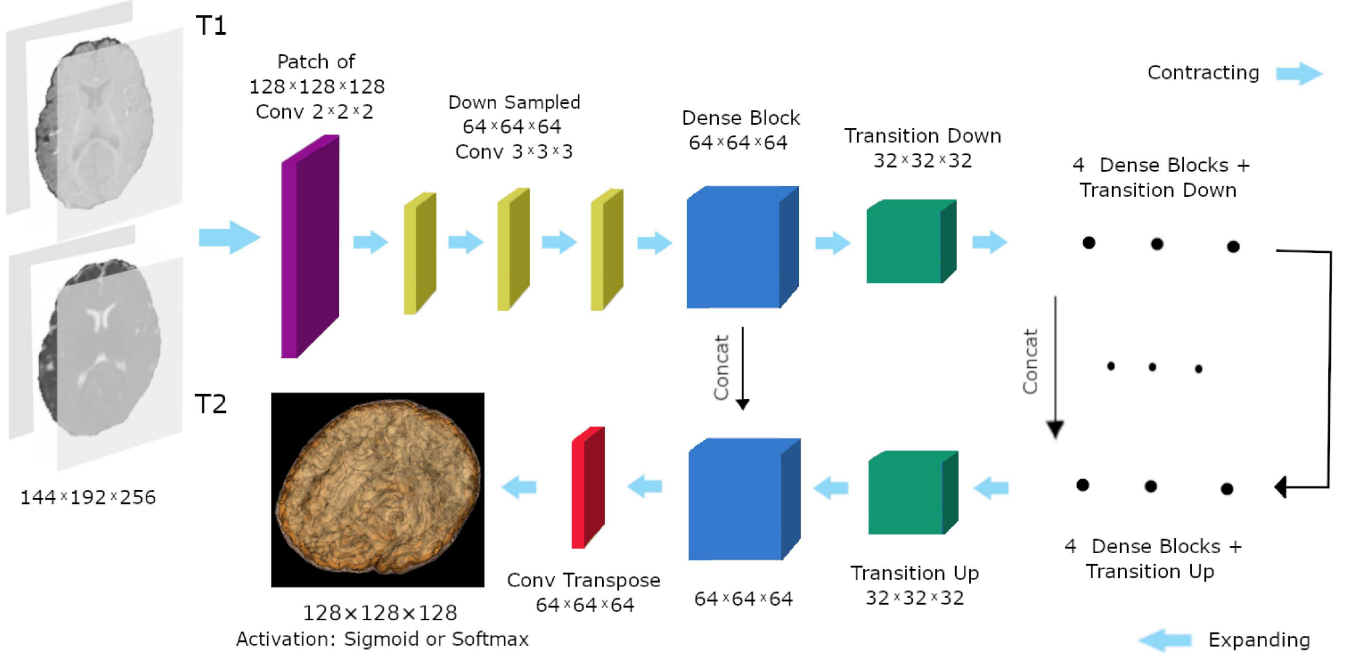


Fig. 2: The 3D FC-DenseNet style architecture in this work; In the first layer, the input patch is downsampled from  $128 \times 128 \times 128$  to  $64 \times 64 \times 64$  using a  $2 \times 2 \times 2$  convolution with stride 2. Before the classification layer, the patch is upsampled from  $64 \times 64 \times 64$  to  $128 \times 128 \times 128$  using a  $2 \times 2 \times 2$  convolution transpose with stride 2. Using this architecture, we do not face any memory issues with large input patches, while maintaining a large field of view.

### 3.2.1. Single-label multi-class

Often in machine learning and deep learning tasks, all labels in a dataset are mutually exclusive which is also the case for the iSeg dataset. This is called a single-label multi-class problem where each voxel can only have one label inside a multi-class environment. One of the most important decisions in a network is the choice of the classification layer. The usual choice for this type of classification for image segmentation is a softmax layer which is a normalized exponential function and a generalization of the logistic function forcing probability values to be in the range of  $[0,1]$  with the total class probability sum of 1:

$$\sigma_z = \frac{e^z}{\sum_{k=1}^n e^k} \quad (3)$$

where  $\sigma$  is the output of the softmax function,  $z$  is the output for label  $z$  before activation,  $k$  is the output for each label  $\in [1, n]$  before activation and  $n$  is the total number of labels. This function assumes dependability of each class to other classes, which is theoretically accurate in the case of iSeg labels (CSF, GM, WM). However, because of human error in generating accurate ground truth labels as well as the isointense specification of GM and WM classes in 6-month infant MRIs, incorporating this theory could result in complications on the border voxels of the two labels where the intensities are most analogous.

Nonetheless, in the single-label approach we trained the network the more popular way and learned all the labels together with a softmax activation function as shown in Figure 3. Then we selected the highest probability class for each voxel. Even though we used an asymmetric loss function to account for data imbalance (discussed later), the network applied the required precision-recall asymmetry mostly on labels with higher level

of occurrence since all the labels were trained together. Therefore, the GM label being the most prevalent class (46.7% of all labeled voxels) would receive higher recall than the other labels (21.84% CSF and 31.45% WM prevalence). Considering both the level of occurrence as well as the isointense aspect of infant brain MRIs, the WM class would receive the least recall among all labels. Therefore, we aimed to exploit other strategies, in particular exclusive independent probability estimation using a multi-label multi-class strategy to better balance the training.

### 3.2.2. Multi-label multi-class

Unlike single-label multi-class problems where voxels can only have one label, in multi-label multi-class problems each voxel has the potential to have multiple labels in a multi-class environment. These types of tasks require prediction of multiple labels per voxel. By using softmax as the activation function, a constant threshold cannot be used because the number of labels is not known in advance and the probabilities are not evenly distributed for every patch or image as demonstrated in Figure 4. Therefore, some sort of binary classification or output function is needed; such as the sigmoid function:

$$\sigma_z = \frac{1}{1 + e^{-z}} \quad (4)$$

which can be written as:

$$\sigma_z = \frac{e^z}{1 + e^z} = \frac{e^z}{e^0 + e^z} \quad (5)$$

where  $\sigma$  is the output of the sigmoid function and  $z$  is the output for label  $z$  before activation. Sigmoid is the special case of softmax for only two classes (i.e. 0 and  $z$ ) which models

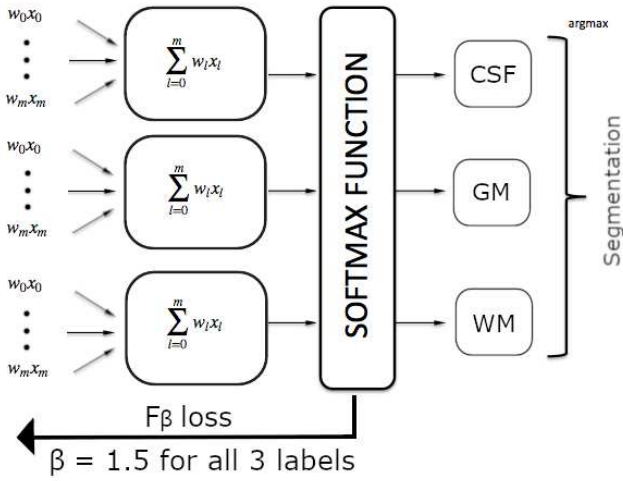


Fig. 3: An example of the Single-label approach with the Softmax activation function and single loss function for all labels.

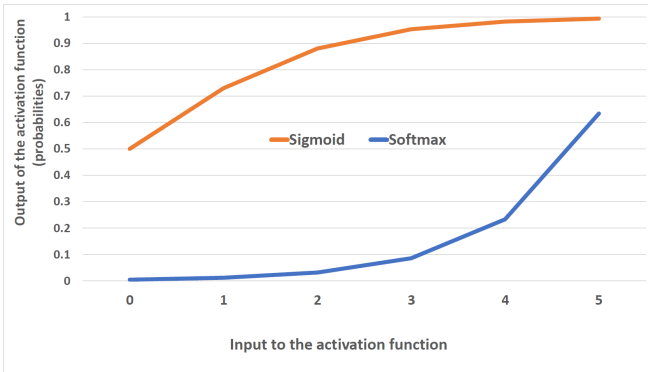


Fig. 4: An example of Sigmoid and Softmax activation functions based on a simple set of [0, 1, 2, 3, 4, 5]. The difference between 4 and 5 in the softmax output is much larger than the sigmoid output. In addition, all of the probabilities will change in softmax if any of the inputs change. Therefore, a constant threshold cannot be used and the scaling of probabilities is not realistic.

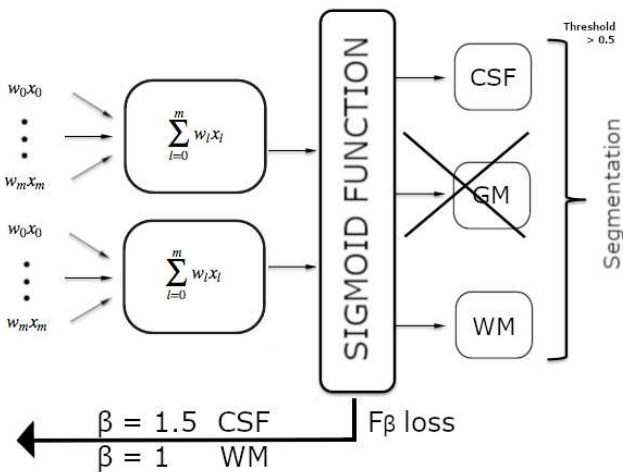


Fig. 5: An example of the Exclusive Multi-label approach with the Sigmoid activation function and multiple loss functions for different labels.

the probability of classes as Bernoulli distributions and independent from other class probabilities as shown in Figure 4. In the multi-label approach, instead of training all the class labels to a probability sum of 1, we scale each class probability separately between [0,1] so later we can use a constant threshold to extract labels (unlike softmax). By using multi-label multi-class approach we also took advantage of different loss functions and hyper-parameters for separate training of each class within the same network. Another advantage is that calculating sigmoid is a less computationally cumbersome task for a processing unit compared to softmax, especially when the number of labels grows.

### 3.2.3. Exclusive multi-label multi-class

Since we decided to use a less complex cost function and to train the class labels independently from each other, there was no reason to train on both of the iso-intense labels, especially when the classes are mutually exclusive. Reducing one of the classes would also help the network focus its attention to one label while eliminating the effect of biased learning towards a class with a larger number of instances as represented in Figure 5. This way, the model has an easier task of learning subtle differences between nearly indistinguishable classes such as GM and WM in iso-intense infant brain MRI segmentation. This can potentially be generalizable to every combination of extremely hard to detect, unbalanced, and mutually exclusive class labels, excluding the one with more occurrences and training on the other while reducing both the number of parameters in the network and the complexity of the training process. To this end, for the iSeg data, we removed GM from the training cycle and trained the CSF class model against non-CSF, and the WM class model in the non-CSF label with differently balanced similarity loss functions discussed in the next subsection. The GM class labels were concluded from the complement of the already predicted CSF and WM labels.

### 3.2.4. Loss function

To better deal with data imbalance, we use an extension of the idea of using similarity loss functions (e.g. the Dice loss function [13]), based on the  $F_\beta$  scores [6]:

$$F_\beta = \frac{(1 + \beta^2) \times \text{precision} \times \text{recall}}{\beta^2 \times \text{precision} + \text{recall}} \quad (6)$$

While Dice similarity is a harmonic mean of precision and recall,  $F_\beta$  allows a balanced similarity function by appropriate choice of the hyper-parameter  $\beta$ . Equation 6 can also be represented as:

$$F_\beta = \quad (7)$$

$$\frac{\text{true positives}}{\text{true positives} + (\frac{\beta^2}{1+\beta^2})\text{false negatives} + (\frac{1}{1+\beta^2})\text{false positives}}$$

The values of  $\beta$  for each class are selected automatically in training based on the ratio of the number of instances per every

other class over the number of instances for all classes being equal to the coefficient of all false negatives in equation 7:

$$\frac{\beta_z^2}{1 + \beta_z^2} = \frac{\sum_{k=1}^n N_k - N_z}{\sum_{k=1}^n N_k} + \lambda \quad (8)$$

which we saw fit regarding the necessary sensitivity rate for each class based on the complement of its portion on all classes.  $\beta_z$  denotes the chosen value for the  $\beta$  hyper-parameter for label  $z$ ,  $N_z$  corresponds to the total number of labels for class  $z$ ,  $n$  is the number of classes and  $\lambda$  is an extra recall hyper-parameter which we set to 0.1 for this experiment. Equation 8 can be represented as:

$$\beta_z = \sqrt{\frac{(1 + \lambda)\sum_{k=1}^n N_k - N_z}{N_z - \lambda\sum_{k=1}^n N_k}} \quad (9)$$

If we assume the  $\lambda$  of 0, then the equation becomes:

$$\beta_z = \sqrt{\frac{\sum_{k=1}^n N_k - N_z}{N_z}} \quad (10)$$

which is the square root of the reverse ratio between the target label and all other labels. Based on the prevalence rate of 21.84% for CSF and 31.45% for WM and  $\lambda = 0.1$ ,  $\beta$  values of 1.5 and 1 were approximated and used for CSF and WM classes, respectively.

### 3.2.5. 3D large patches and patch prediction fusion

Rather than training on full-size, two-channel (T1- and T2-weighted MRI) input images, we extracted and used large 3D two-channel image patches as inputs and augmented the training data at the level of large patches. This had several advantages including efficient use of memory, intrinsic data augmentation, and the design of an image size-independent model. Previously in the Network Architecture section, we mentioned that large patches of  $128 \times 128 \times 128$  are selected from the image and are immediately downsampled to  $64 \times 64 \times 64$  to preserve higher receptive field while adapting to GPU memory restrictions. Nonetheless, due to limited effective receptive field of input patches (even with large patches), accuracy near patch borders was relatively low mainly because of the effective receptive field near the patch borders. To circumvent this problem while fusing patch predictions in both training and testing, we exploited a weighted soft voting approach [6] using second-order spline functions placed at the center of patches. Patches were selected for prediction using 50% overlaps. Each patch was rotated 180 degrees once in each direction for augmentation in training, and the final result was calculated through the fusion of predictions by all overlapping patches and their augmentations.

### 3.3. Experimental design

We trained and tested our 3D FC-DenseNet with  $F_\beta$  loss layer to segment isointense infant brains. T1- and T2-weighted MRI of 10 subjects were used as input, where we used five-fold cross-validation in training. There was not any pre-processing

involved as the images were already skull-stripped and registered. The two MRI images of each subject were normalized through separately dividing each voxel value by the mean of non-zero voxels in each image. This way the whole brain (excluding background) in each modality was normalized to unit mean. Our 3D FC-DenseNet was trained end-to-end. Cost minimization on 2,500 epochs was performed using ADAM optimizer [12] with an initial learning rate of 0.0005 multiplied by 0.9 every 500 steps. The training time for this network was approximately 14 hours on a workstation with Nvidia Geforce GTX1080 GPU.

Validation and test volumes were segmented using feed-forward through the network. The output of the last convolutional layer with softmax non-linearity consisted of a probability map for CSF, GM and WM tissues. For the sigmoid version of the network, it contained only the CSF and WM tissues. In the softmax approach (single-label multi-class), the class with maximum probability among all classes was selected as the segmentation result for each voxel, while in the sigmoid approach (exclusive multi-label multi-class) voxels with computed probabilities  $\geq 0.5$  were considered to belong to the specific tissue class (CSF or WM) and those with probabilities  $< 0.5$  were considered non tissue. For voxels with both CSF and WM probabilities of  $\geq 0.5$  the class with higher probability was selected. Finally, GM labels were generated based on the compliment of predicted CSF and WM class labels.

### 3.4. Evaluation metrics

To evaluate and compare the performance of the network against state-of-the-art in isointense infant brain segmentation, we report Dice Similarity Coefficient (DSC):

$$\text{DSC} = \frac{2|P \cap R|}{|P| + |R|} = \frac{2TP}{2TP + FP + FN} \quad (11)$$

which is equivalent to the  $F_1$  score calculated by setting  $\beta = 1$  in Equation 7. TP, FP, and FN are the true positive, false positive, and false negative rates, respectively; and P and R are the predicted and ground truth labels, respectively. In the iSeg challenge, in addition to the DSC score, Modified Hausdorff distance (MHD):

$$\text{MHD} = \max\{\max_{q \in R} d(q, P), \max_{q \in P} d(q, R)\} \quad (12)$$

and Average Surface Distance (ASD):

$$\text{ASD} = \frac{1}{|R|} \sum_{p \in R} d(p, P) \quad (13)$$

were also reported in the test set results, where  $d(q, P)$  denotes the point-to-set distance:  $d(q, P) = \min_{p \in P} \|q - p\|$ , with  $\|\cdot\|$  presenting the Euclidean distance and  $|\cdot|$  denoting the cardinality of a set.

## 4. Results

To evaluate the effect of our proposed exclusive multi-label multi-class training strategy compared to single-label methods,



Table 1: Average performance metrics (on the validation sets) of state-of-the-art methods tested on the 2017 iSeg challenge dataset. The best values for each metric have been highlighted in bold. The top three methods in the table are derived from [2], therefore the training process and cross validation folds may be different and can not be directly compared to the bottom two methods. Comparable results on the official test set are shown in Table 2.

Method	DSC			Depth	Params
	CSF	GM	WM		
3D Unet [4]	94.44	90.73	89.57	18	19M
DenseVoxNet [21]	93.71	88.51	85.46	32	4.34M
DenseSeg - MSK SKKU [2]	<b>94.69</b>	<b>91.57</b>	<b>91.25</b>	47	1.55M
3D FC-DenseNet Single	94.86	91.18	89.27	60	1.5M
3D FC-DenseNet (Exc) Multi	<b>95.19</b>	<b>91.79</b>	<b>90.37</b>	60	1.4M

Table 2: Performance metrics (on the test set) of the top ranking teams in the 2017 iSeg challenge. The best values for each metric have been highlighted in bold. Our method outperformed the first ranking team [2] at the time of the challenge and stands, overall, in the first place among all first and second round submissions through September 2018 (<http://iseg2017.web.unc.edu/evaluation-on-the-second-round-submission/>).

Teams (Published)	CSF			GM			WM		
	DSC	MHD	ASD	DSC	MHD	ASD	DSC	MHD	ASD
BCH CRL IMAGINE (ours)	<b>96.0</b>	<b>8.85</b>	<b>0.11</b>	<b>92.6</b>	9.55	<b>0.31</b>	<b>90.7</b>	7.1	<b>0.36</b>
MSL SKKU (2nd round)[2]	95.8	9.11	0.116	92.3	6.0	0.32	90.4	6.62	0.375
MSL SKKU (1st round)	95.8	9.07	0.116	91.9	<b>5.98</b>	0.33	90.1	<b>6.44</b>	0.39
LIVIA (2nd round) [5]	95.6	9.42	0.12	92.0	5.75	0.33	90.1	6.66	0.38
LIVIA (1st round)	95.7	9.03	0.138	91.9	6.42	0.34	89.7	6.98	0.38
Bern IPMI	95.4	9.62	0.127	91.6	6.45	0.34	89.6	6.78	0.4
nic vicorob	95.1	9.18	0.137	91.0	7.65	0.37	88.5	7.15	0.43

we trained our FCN with single- and multi-label designs and calculated cross-validation DSC. The characteristics and performance metrics of our two trained models are compared with other methods (also tested on the iSeg challenge validation sets), reported in [2], in Table 1; however, the DSC results of the top part of the table and our results in the bottom part are not directly comparable because of possible differences in cross-validation sets. The actual comparison based on official iSeg test set results are reported in Table 2.

Our 3D FC-DenseNet architecture is deeper than the rest and has less number of parameters. The performance metrics of our exclusive multi-label model (on the iSeg challenge final test set) are reported in Table 2. The results show that our method outperformed all methods that were reported at the time of the challenge as well as both the DenseNet based methods of DenseSeg [2] and HyperDenseNet [5] that overall ranked 1<sup>st</sup> and 2<sup>nd</sup> in both first and second rounds of submission. According to the performance metrics reported on the iSeg results page, our method performed better than all other methods. This improved performance is attributed to both our improved network architecture and its training which made a balance between precision and recall controlled by the parameters of our  $F_\beta$  loss function leading to different training conditions for different labels compared to a single-label training for all labels using the cross-entropy or dice loss functions [2, 5].

Figure 6 shows the prediction results of a subject from one of the validation folds for our two training methods compared to the ground truth. The best results were achieved by our exclusive multi-label model with better DSC scores on all class labels, and visually-observed improvements in segmentation.

## 5. Conclusion

We introduced a new deep densely connected network [9] based on [2, 10], called 3D FC-DenseNet that has more depth and less parameters than its predecessors, while having the capability of including 4 times the regular patch sizes ( $128 \times 128 \times 128$  vs  $64 \times 64 \times 64$ ) due to its early downsampling and late upsampling layers. To train this deep network we used similarity  $F_\beta$  loss functions that generalized the Dice similarity, and achieved better trade-off between precision and recall in segmentation. We designed two pipelines for training, a single-label and an exclusive multi-label procedure. Experimental results in 6-month infant brain segmentation show that performance evaluation metrics (on the validation set) improved by using exclusive multi-label rather than single-label training. The loss function was designed to weigh recall higher than precision (at  $\beta = 1.5$ ) for CSF, while using equal precision-recall ratio ( $\beta = 1$ ) for WM labels against GM, based on class prevalence in the training set. Official test results based on DSC, MHD, and ASD scores on the iSeg challenge data indicate that our method performed very well compared to the latest results in isointense infant brain MRI segmentation, improving the results of all previous DenseNet-based methods [2, 5].

## 6. Acknowledgements

This study was supported in part by a Technological Innovations in Neuroscience Award from the McKnight Foundation and National Institutes of Health grants R01 EB018988 and R01 NS079788.

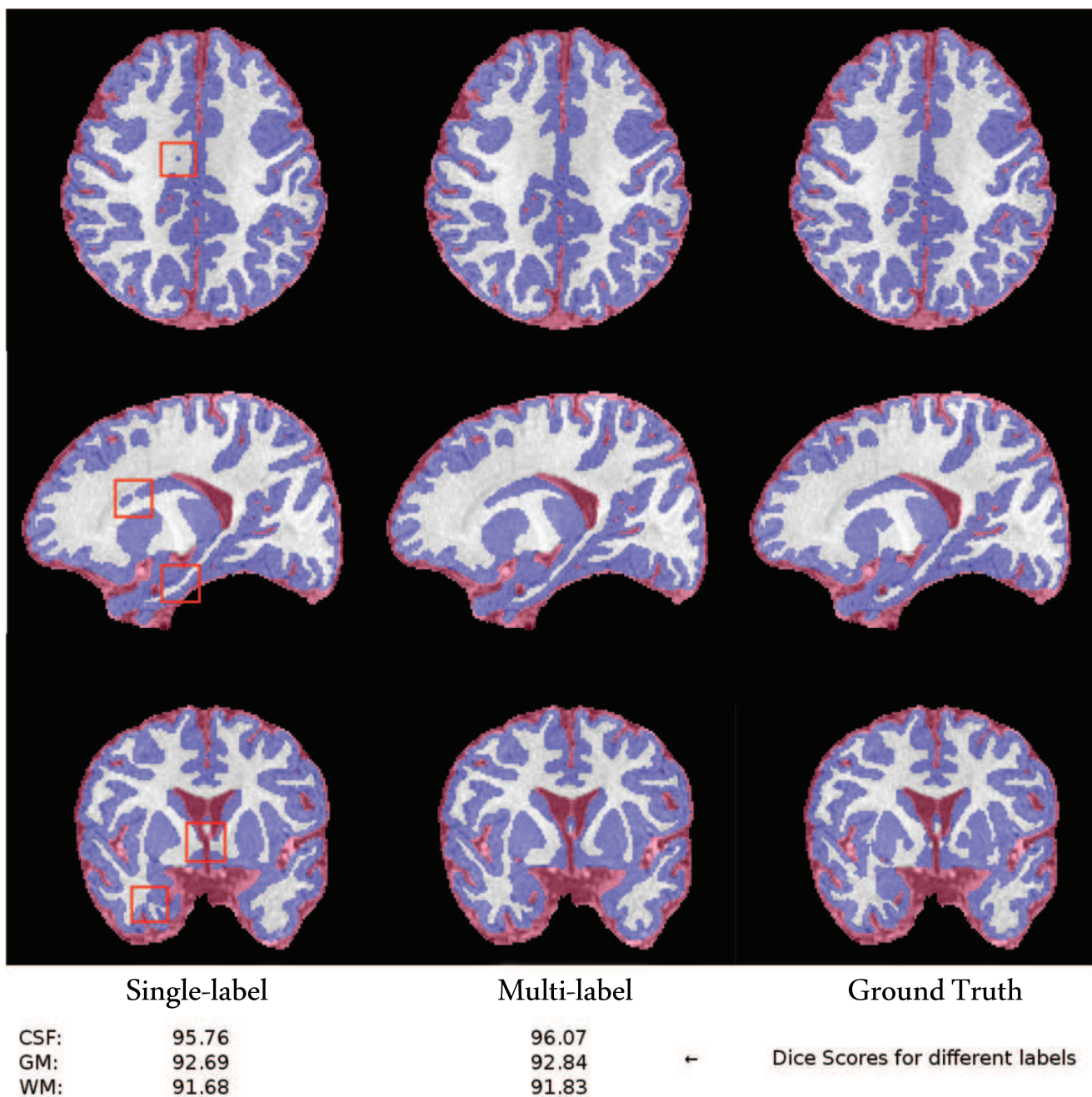


Fig. 6: An example of Single-label and Exclusive Multi-label brain tissue segmentation of subject 1 in the validation set. Dice scores for each class label are shown below each image. The red squares highlight some areas of difference between the two approaches.



## References

- convolutional neural networks for multi-modality iso-intense infant brain image segmentation. *NeuroImage* 108, 214–224 (2015)
- [1] Brosch, T., Yoo, Y., Tang, L.Y., Li, D.K., Traboulsee, A., Tam, R.: Deep convolutional encoder networks for multiple sclerosis lesion segmentation. In: *International Conference on Medical Image Computing and Computer-Assisted Intervention*. pp. 3–11. Springer (2015)
  - [2] Bui, T.D., Shin, J., Moon, T.: 3d densely convolutional networks for volumetric segmentation. *arXiv preprint arXiv:1709.03199* (2017)
  - [3] Chen, H., Dou, Q., Yu, L., Qin, J., Heng, P.A.: VoxResNet: Deep voxelwise residual networks for brain segmentation from 3D MR images. *NeuroImage* (2017)
  - [4] Çiçek, Ö., Abdulkadir, A., Lienkamp, S.S., Brox, T., Ronneberger, O.: 3D U-Net: learning dense volumetric segmentation from sparse annotation. In: *International Conference on Medical Image Computing and Computer-Assisted Intervention*. pp. 424–432. Springer (2016)
  - [5] Dolz, J., Gopinath, K., Yuan, J., Lombaert, H., Desrosiers, C., Ben Ayed, I.: Hyperdense-net: A hyper-densely connected cnn for multi-modal image segmentation. *arXiv preprint arXiv:1804.02967* (2018)
  - [6] Hashemi, S.R., Salehi, S.S.M., Erdogmus, D., Prabhu, S.P., Warfield, S.K., Gholipour, A.: Asymmetric similarity loss function to balance precision and recall in highly unbalanced deep medical image segmentation. *arXiv preprint arXiv:1803.11078* (2018)
  - [7] Havaei, M., Davy, A., Warde-Farley, D., Biard, A., Courville, A., Bengio, Y., Pal, C., Jodoin, P.M., Larochelle, H.: Brain tumor segmentation with deep neural networks. *Medical image analysis* 35, 18–31 (2017)
  - [8] He, K., Zhang, X., Ren, S., Sun, J.: Deep residual learning for image recognition. *IEEE Conference on Computer Vision and Pattern Recognition (CVPR)* (2016)
  - [9] Huang, G., Liu, Z., van der Maaten, L., Weinberger, K.Q.: Densely connected convolutional networks. *Proceedings of the IEEE Conference on Computer Vision and Pattern Recognition* (2017)
  - [10] Jegou, S., Drozdal, M., Vazquez, D., Romero, A., Bengio, Y.: The one hundred layers tiramisù: Fully convolutional densenets for semantic segmentation. *arXiv preprint arXiv:1611.09326* (2017)
  - [11] Kamnitsas, K., Ledig, C., Newcombe, V., Simpson, J., Kane, A., Menon, D., Rueckert, D., Glocker, B.: Efficient multi-scale 3D CNN with fully connected CRF for accurate brain lesion segmentation. *Medical Image Analysis* 36, 61–78 (2017)
  - [12] Kingma, D., Ba, J.: Adam: A method for stochastic optimization. *arXiv preprint arXiv:1412.6980* (2014)
  - [13] Milletari, F., Navab, N., Ahmadi, S.A.: V-net: Fully convolutional neural networks for volumetric medical image segmentation. In: *3D Vision (3DV), 2016 Fourth International Conference on*. pp. 565–571. IEEE (2016)
  - [14] Moeskops, P., Viergever, M.A., Mendrik, A.M., de Vries, L.S., Benders, M.J., Išgum, I.: Automatic segmentation of MR brain images with a convolutional neural network. *IEEE transactions on medical imaging* 35(5), 1252–1261 (2016)
  - [15] Pereira, S., Pinto, A., Alves, V., Silva, C.A.: Brain tumor segmentation using convolutional neural networks in MRI images. *IEEE transactions on medical imaging* 35(5), 1240–1251 (2016)
  - [16] Salehi, S.S.M., Erdogmus, D., Gholipour, A.: Auto-context convolutional neural network (Auto-Net) for brain extraction in magnetic resonance imaging. *IEEE Transactions on Medical Imaging* (2017)
  - [17] Salehi, S.S.M., Hashemi, S.R., Velasco-Annis, C., Quaalam, A., Estroff, J.A., Erdogmus, D., Warfield, S.K., Gholipour, A.: Real-time automatic fetal brain extraction in fetal MRI by deep learning. *IEEE International Symposium on Biomedical Imaging* (2018)
  - [18] Valverde, S., Cabezas, M., Roura, E., González-Villà, S., Pareto, D., Vilanova, J.C., Ramió-Torrentà, L., Rovira, À., Oliver, A., Lladó, X.: Improving automated multiple sclerosis lesion segmentation with a cascaded 3D convolutional neural network approach. *NeuroImage* 155, 159–168 (2017)
  - [19] Wachinger, C., Reuter, M., Klein, T.: DeepNAT: Deep convolutional neural network for segmenting neuroanatomy. *NeuroImage* (2017)
  - [20] Wang, L., Shi, F., Yap, P.T., Lin, W., Gilmore, J.H., Shen, D.: Longitudinally guided level sets for consistent tissue segmentation of neonates. *Human Brain Mapping* 34(7), 956–972 (2013)
  - [21] Yu, L., Cheng, J.Z., Dou, Q., Yang, X., Chen, H., Qin, J., Heng, P.A.: Automatic 3d cardiovascular MRI segmentation with densely-connected volumetric convnets. *MICCAI* (2017)
  - [22] Zhang, W., Li, R., Deng, H., Wang, L., Lin, W., Ji, S., Shen, D.: Deep